

Tomoaki Nakazono et al. / *Neuroscience xxx (xxxx) xxx–xxx*

## Enhanced Theta and High-Gamma Coupling during Late Stage of Rule Switching Task in Rat Hippocampus

Tomoaki Nakazono,<sup>ab,1</sup> Susumu Takahashi<sup>c</sup> and Yoshio Sakurai<sup>ab</sup>

<sup>a</sup>Laboratory of Neural Information, Graduate School of Brain Science, Doshisha University, Kyoto, Japan

<sup>b</sup>Department of Psychology, Graduate School of Letters, Kyoto University, Kyoto, Japan

<sup>c</sup>Laboratory of Cognitive and Behavioral Neuroscience, Graduate School of Brain Science, Doshisha University, Kyoto, Japan

**Abstract**—Hippocampal oscillations, particularly theta (6–12 Hz) and gamma (30–90 Hz) frequency bands, play an important role in several cognitive functions. Theta and gamma oscillations show cross-frequency coupling (CFC), wherein the phase of theta rhythm modulates the amplitude of the gamma oscillation, and this CFC is believed to reflect cell assembly dynamics in cognitive processes. Previous studies have reported that CFC strength correlates with the learning process. However, details on these dynamic correlations have not been elucidated. In the present study, we analyzed local field potentials recorded from the rat hippocampus during the learning of a rule-switching task. The modulation index, an index of the CFC strength, became higher in rule-guided behavior than in the no rule condition. The enhanced coupling between theta and high-gamma oscillations (60–90 Hz) changed during the late stage of learning. In contrast, the coupling between theta and low-gamma oscillations (30–60 Hz) did not show any changes during learning. These results suggest that the coupling between theta and gamma bands occurs during rule learning and that high- and low-gamma bands play different roles in rule switching. © 2019 IBRO. Published by Elsevier Ltd. All rights reserved.

**Key words:** learning, rule-switching, hippocampus, rat, cross-frequency coupling, theta–gamma coupling.

### INTRODUCTION

In daily life, animals must continue to update knowledge about the surrounding environment, find better strategies through a trial and error process, and improve their behavior to maximize gain. During such learning process, information coding in our brain should change quickly and flexibly.

Cell assembly hypothesis is thought to be the mechanism underlying the plasticity of our brain (Hebb, 1949). According to this hypothesis, synchronized groups of neurons underlie information processing (Sakurai, 1999; Harris, 2005; Buzsáki, 2010). Such neuronal groups can change their members and process different information flexibly. Indeed, the synchronized firings of hippocampal neurons are differentially modulated by reference and working memory demand (Sakurai, 1996, 2002) and improve the prediction of place cell activity pattern from the neuronal ensemble activity (Harris et al., 2003). The hippocampus is thought to play an important role in such learning process; however, the detailed

dynamics of neuronal populations in the hippocampus remain unclear.

Because local field potentials (LFPs) are thought to perform the necessary temporal coordination of neuronal spikes in neuronal circuitry, these can be used to study the mechanisms in the hippocampus. Several lines of evidence suggest that theta (6–12 Hz) and gamma (30–90 Hz) oscillations participate in the mechanisms underlying cell assembly (Lisman and Jensen, 2013). These two oscillations are prominent rhythms in the rodent hippocampus and play different roles. Gamma oscillations modulate the synchronized firing of neuronal populations and help to coordinate groups of neurons into functional assemblies, that is, cell assemblies (Fries et al., 2001; Harris et al., 2003). In contrast, theta oscillation is thought to be a rhythm that binds sequential events into an episode-like information (O'Keefe and Dostrovsky, 1971; Dragoi and Buzsáki, 2006; Terada et al., 2017). Although each type of oscillation has distinct functions, these two rhythms show strong interactions (cross-frequency coupling, CFC). In rodent hippocampus, a prominent phenomenon in CFC is the modulation of gamma oscillation amplitude by theta oscillation phases (phase-amplitude coupling). This coupling is thought to be a mechanism that binds local cell assemblies, which are organized by gamma oscillations, to the larger assemblies, by theta oscillation (Canolty et al.,

\*Corresponding author at: Laboratory of Neural Information, Graduate School of Brain Science, Doshisha University, Kyoto, Japan.  
E-mail address: [tnakazono@fmu.ac.jp](mailto:tnakazono@fmu.ac.jp) (Tomoaki Nakazono).

<sup>1</sup> Present affiliation: Department of Systems Neuroscience, School of Medicine, Fukushima Medical University, Fukushima, Japan.

2010; Lisman and Jensen, 2013). Such CFC was observed across several brain regions of the rodent hippocampus (Tort et al., 2008, 2009; Colgin et al., 2009; Shirvankar et al., 2010; Takahashi et al., 2014; Amemiya and Redish, 2018; Lopes-dos-Santos et al., 2018), entorhinal cortex (Yamamoto et al., 2014), prefrontal cortex (Li et al., 2012), orbitofrontal cortex (OFC) (van Wingerden et al., 2014), and motor cortex (Igarashi et al., 2013). Electroecortigraphy, electroencephalography, and direct recording data from the human brain also showed CFC (Canolty et al., 2006; Kajihara et al., 2015; Mizuhara et al., 2015; Zheng et al., 2017). These studies suggest that the CFC reflects a common mechanism for dynamic information processing in the brain and coordinates cell assembly dynamics.

Studies have reported that the CFC strength changes during the learning process (Tort et al., 2008, 2009; Nishida et al., 2014; van Wingerden et al., 2014). However, there are still questions related to these studies that remain to be

answered. First, the effect of reward on CFC is unclear. Because the probability of receiving a reward is increased during learning, CFC could be affected by changes in the reward magnitude. Second, it is unclear if CFC reflects the process of trial and error or the acquisition of new knowledge. Third, it remains to be determined if there are differences in the gamma types coupled with theta in the learning process even in non-spatial task.

In this study, to address these questions, we introduced a rule-switching task in the rats (Fig. 1). In this rule-switching task design, the correct choice can be changed even when sensory information is the same (Fig. 1C). This design allowed us to exclude the effects of sensory input from the learning process. We recorded LFPs in the hippocampus of rats while they performed this task.

To answer the first question, we have used a yoked control design, which consists of a reward schedule that matches the experimental conditions but was irrelevant to the animal's

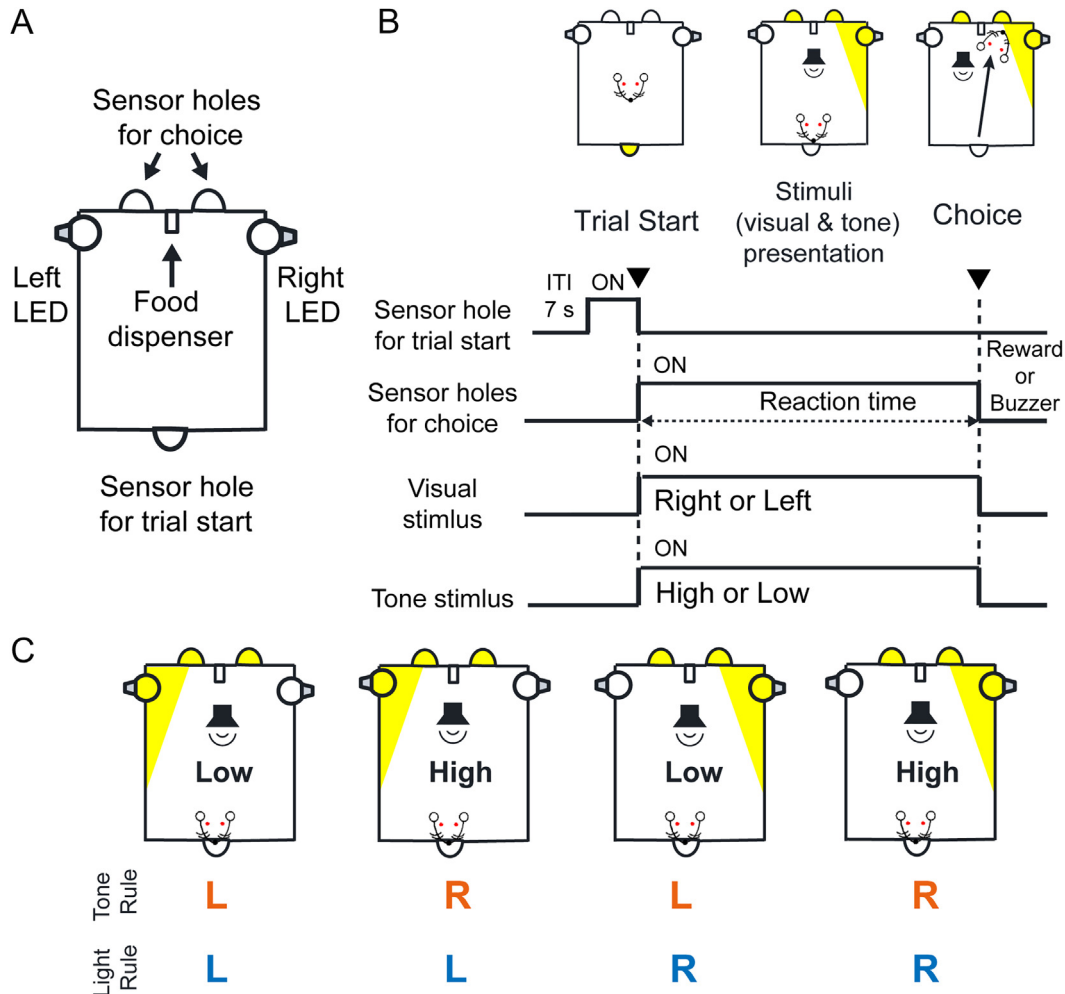


**Fig. 1. Rule switching task.** (A) Illustration of the operant chamber. One wall had the sensor holes for choice and the food dispenser, and the wall on the other side had the sensor hole for detecting the trial start. (B) The sequence of events for the rule switching task. After the trial started (top-left), both visual and tone stimuli were presented simultaneously (top-middle). Rats had to choose the correct hole by following one of the stimuli to receive a reward (top-right). However, there was no cue to indicate which stimulus they should select. Therefore, rats had to determine the rule of which stimulus was correct through trial and error learning. Bottom, illustration of the sequence of events. (C) The four combinations of light and tone stimuli and the correct responses to the right (R) or left (L) hole (red: following the tone rule, blue: following the light rule). (For interpretation of the references to color in this figure legend, the reader is referred to the web version of this article.)

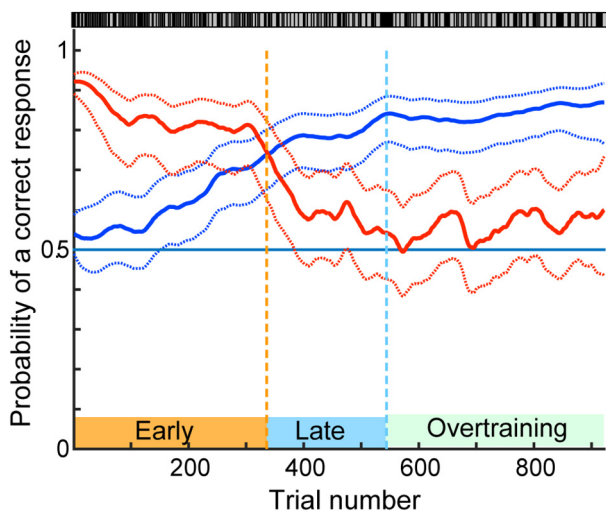


**Fig. 2. An example of learning process.** The red line shows the estimated probability of a correct response to the previous rule as a function of trial number, whereas the blue line is that for the new rule. The dotted lines show the upper and lower confidence intervals (95%) for the estimated probabilities. The incorrect and correct responses to the new rule are shown with black and gray marks above the panels, respectively. An orange dotted line shows the point at which a correct rate for the new rule exceeded that for previous rule. A pale blue dotted line shows the end point of a learning trial. (For interpretation of the references to color in this figure legend, the reader is referred to the web version of this article.)

response. This control design allowed us to isolate the effect of the reward from those of the learning process. To address the second question, we have separated the learning process into an early stage, i.e., when the animals still follow the previous rule, and a late stage, i.e., when the same animals learn the new rule.

To answer our third question, it should be noted that there are at least two types of gamma oscillations in the hippocampus (Colgin et al., 2009; Belluscio et al., 2012; Lopes-dos-Santos et al., 2018): low-frequency and high-frequency gamma oscillations. Previous studies suggested that they differ in regard to cognitive roles, especially memory (Colgin et al., 2009; Bieri et al., 2014; Zheng et al., 2015a; Lopes-dos-Santos et al., 2018). For instance, low-frequency gamma is thought to contribute to memory recall, and high-frequency gamma is thought to contribute to memory encoding. Therefore, we have analyzed the CFC dynamics between theta and low-frequency gamma oscillations and between theta and high-frequency gamma oscillations in the hippocampal CA1 area of rats during the rule switching task performance.

## EXPERIMENTAL PROCEDURES

### Subjects

Twelve male Wistar albino rats (Shimizu Laboratory Supplies, Kyoto, Japan), each weighing 500–580 g at the time of the experiment, were housed in 250 × 150 × 240-mm cages on a 12–12-h light–dark cycle. Data from only six rats were used for the behavioral analysis because of the significant noise in the recorded signals. The data from the

remaining six rats were used for both, the LFP and behavioral analyses. All rats were gently handled, allowed *ad libitum* access to water, and provided with sufficient rodent chow 2–3 h after daily training or recording sessions to maintain 80–90% of their starting body weight. All experimental procedures were performed in accordance with the Regulation on Animal Experimentation Guidelines of Kyoto University (2007) and were approved by the Animal Research Committee of Kyoto University.

### Apparatus

Rats were trained on a behavioral task in a dim, sound-attenuated, electrically shielded box (Japan Shield Enclosure, Osaka, Japan) that included a 175 × 320 × 450-mm operant chamber (O'HARA&CO. LTD, Tokyo, Japan) (Fig. 1A). One wall of the chamber had three illuminated sensor holes, which were used to detect the nose-poke behavior of rats. The sensors were 15 mm in diameter and were horizontally placed 60 mm above the floor. Access to the three holes was controlled using a guillotine door in front of each hole. However, only the right and left holes were used for the task. The opposite wall of the chamber also had three illuminated sensor holes. On this side, only the center hole was used for the task. A food dispenser located behind the wall delivered 25 mg of food pellets to a food chamber located in the center of the wall and 10 mm above the floor. The dispenser delivered pellets coupled with an intermittent low buzzer tone (reward tone). This buzzer was also located behind the wall. Another buzzer, located 400 mm above the floor of the wall, delivered a continuous buzzer tone when the rats made erroneous responses (error tone). Visual stimuli were presented on the left or right wall using a light-emitting diode (LED). Tone stimuli consisting of two pure tones (2 or 10 kHz) of approximately 70 dB sound pressure level were presented via a loudspeaker (150 mm in diameter) located 300 mm above the top of the operant chamber. The task was controlled, and behavioral data were recorded using a personal computer (NEC, Tokyo, Japan).

### Behavioral task

Each rat was trained for the rule switching task, which was largely modified from our previous study (Sakata et al., 2002). Before each trial, the guillotine door was closed. The inter-trial interval (ITI) was 7 s, after which, the center hole of the opposite side wall was illuminated. A trial started when a rat poked his nose in the illuminated center hole. After the trial started, the light of the center hole was switched off, while visual and tone stimuli were presented simultaneously. At the same time, the guillotine door opened and the two holes (the left and right holes) on the same side of the wall became illuminated and accessible. The rats learned to select one of the two illuminated holes by following one of the two types of cue stimuli presented at the same time to get a food reward through the food dispenser (Fig. 1B). Both visual and tone stimuli were continued until the rat poked his nose in either of the hole. However, only one of the cue types was valid, and the other cue type was used as a distractor. The cue type indicating the correct hole was fixed throughout a session,

and this valid cue type was referred to as the “rule” for the task. For the “light rule”, the hole on the same side with the visual stimuli was the correct one. For the “tone rule”, the high tone (10 kHz) meant that the right hole was correct, while the low tone (2 kHz) meant that the left hole was correct. Each of the four combinations of light and tone stimuli was presented in a random order, and the validity of the light and tone stimuli for the correct responses was consistent for 50% of the trials (Match trials) and inconsistent for the other 50% of the trials (Non-Match trials) (Fig. 1C). An incorrect choice closed the door, produced a 1-s buzzer noise, and was followed by a series of correction trials until the rat chose the correct hole. No data were recorded during the correction trials. Each training or recording session continued for a maximum of 160 trials, excluding the correction trials, or until 90 min elapsed.

### Experiment schedule

Learning was considered complete once the rats' performance reached both of the two following criteria: (1) a lower 95% confidence interval for the estimated learning curve of the previous rule below 0.5; and (2) more than 15 consecutive correct trials. Learning curves were estimated using the method previously described (Smith et al., 2004). At least one session was completed after learning as an overtraining session (Fig. 2). The data recorded from the first overtraining session were used for analysis.

After the overtraining session, the rule was switched. The rats learned the new rule through trial and error because there was no cue to indicate the rule switch. All rats started the training of the ruleswitching task with a tone rule as it was more difficult to learn than the light rule. Sessions with a tone rule were termed “tone sessions” and sessions with a light rule were termed “light sessions”. The numbers of rule switches varied for each rat.

After the rule switching task experiment, a yoked control experiment was performed, whereby the sequence of trials

was the same as that for the rule switching experiment, and both light and tone stimuli were presented randomly. However, rewards were delivered using the history of reward delivery for the first rule switching learning (tone rule to light rule) regardless of the choice response of the rat. In other words, the yoked control experiment had no rule even though it had similar sensory inputs with two experimental conditions. This yoked control session was termed “control session”. The control experiment was performed after the overtraining session of the tone rule learning.

To analyze the behavioral data, we calculated the correct rates for the tone rule and light rule, choice bias, and reaction time. For example, when a correct rate for the tone rule was 100%, a correct rate for the light rule was 50% because the indications for tone and light stimuli were the same for 50% of all trials. We defined choice bias as a higher correct rate of the two rules for the non-match trials. This index was calculated to examine how the rats obeyed one rule and ignored the other rule. Reaction time was defined as the time from the trial start to the selection of a choice.

### Electrode construction, implantation, and recording

LFP recordings were conducted with three bundles of four tungsten microwires (HML-coated 12.7  $\mu\text{m}$  in diameter; California Fine Wire, Grover Beach, CA, USA) as a tetrode. The microwires were mounted in a 25-mm length 33-gauge stainless-steel cannula (Small Parts, Miami, FL, USA) with a protruding tip length of 500  $\mu\text{m}$ . These cannulas were used as a reference. The tips were cut at right angles with sharp surgical scissors. The tip impedance was approximately 400 k $\Omega$  (at 1 kHz). Cannulas were attached in a row to construct an array of tetrodes, with a center-to-center spacing of 500  $\mu\text{m}$  between the cannulas. The array of tetrodes was mounted on a microdrive assembly (McNaughton et al., 1989) that was designed to allow fine adjustment of the electrode position in the dorso-ventral direction during a chronic

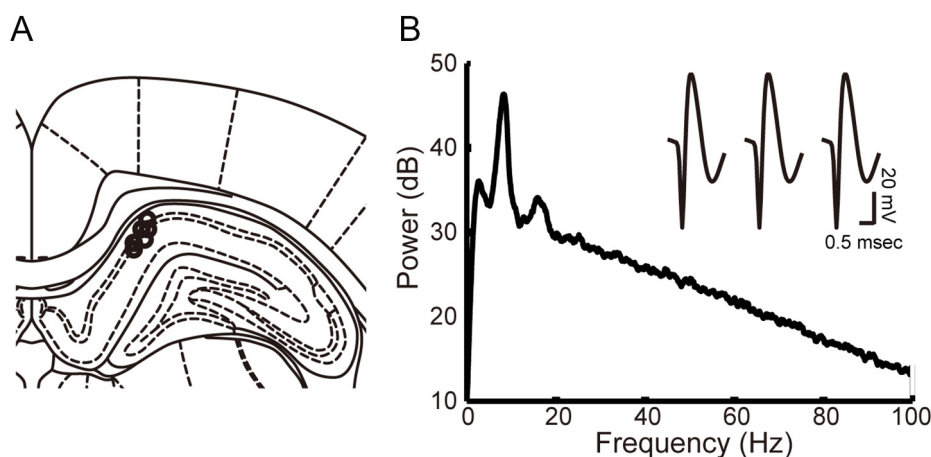


**Fig. 3. Examples of LFP power spectrum and unit waveforms.** (A) Tetrode recording sites in hippocampal CA1 (bregma:  $-3.8$  mm). (B) A multitaper spectrum example for an LFP recorded from one rat. Inset, example waveforms of a putative pyramidal cell. Unit activities were recorded from three tetrode channels, and another channel was used for LFP recording.

recording. After completion of the first learning of the rule switching task with the tone rule, each rat was anesthetized with isoflurane (0.5–3%), and the microdrive with electrodes was chronically fixed to the skull above the right hippocampal CA1 region (AP –3.8 mm, ML 2.0 mm, DV 1.0 mm) (Fig. 3A). The craniotomies were filled with white petrolatum to a level slightly above the point where the tetrodes exited the skull surface. After the supports of the microdrives and canulas were coated with a thin film of white petrolatum, the entire assembly was embedded on the skull surface using dental cement. The rats were allowed to recover for approximately 1 week following the implantation surgery. We lowered the electrodes post-surgery to obtain stable long-term recordings. Head stages containing 24 field-effect transistors (2SK371, Toshiba, Tokyo, Japan) set as source followers were used to connect a 24-channel plastic connector cemented to the animal's head. LFPs were amplified, filtered (0.5–300 Hz), and recorded at 20 kHz on a custom-made personal computer with a 24-channel A/D converter (16-bit resolution; Contec Co. Ltd., Osaka, Japan). The tetrodes were slowly advanced towards the hippocampus while unit activity and LFP data were monitored. For the LFP recording, the most prominent tetrode was used for analysis. We used one recording channel for LFP recording and the other three channels for unit recording. Recorded spike trains were sorted to isolate individual neuronal activities using independent component analysis (ICA) and k-means clustering called ICsort (Takahashi et al., 2003a, 2003b). We selected recording positions (pyramidal cell layer of the dorsal CA1) depending on the LFP power of the theta band and multiple single unit activities of putative pyramidal cells (Fig. 3B). We judged putative pyramidal cells based on their wide spike shape (mean width > 0.25 ms) and low average firing rate (<5 Hz) (Fig. 3B). The recording points were fixed throughout experiments. The unit activity data were only used for this purpose and were not analyzed. The data from trials with poor signal-to-noise ratio were excluded from the analysis. We used data from both correct and error trials, to examine LFP dynamics throughout the learning process.

### Calculation of the power of LFPs

We used the Chronux toolbox (<http://www.chronux.org>) (Mitra and Bokil, 2007) and custom-written programs in MATLAB (MathWorks, Natick, MA, USA) for our multi-taper Fourier analysis. Before analysis, the direct current offsets, slowly changing components, and 60-Hz line noise were removed from the LFP data by applying the locdetrend and rmlines functions in the Chronux toolbox. The theta, low gamma, and high gamma frequency bands were defined as 6–12, 30–60, and 60–90 Hz, respectively. To calculate the power spectrum, the Chronux function (mtpspecgramc.m) was used with the following parameters: 1-s window size, 50-ms time step, time-bandwidth product of 5, and taper count of 9. The power spectra were normalized using the mean of the power during the ITI (–5 s to –1 s from trial start). We defined four events: before 1 s from trial start (PRE), after 1 s from trial start (RUN1), before 1 s from choice (RUN2), and after 1 s from choice (POST). In

statistical test, we calculated mean LFP powers for each animal in three conditions (tone rule, light rule, and control condition) and four trial events (PRE, RUN1, RUN2, and POST) and performed two-way repeated measures ANOVA.

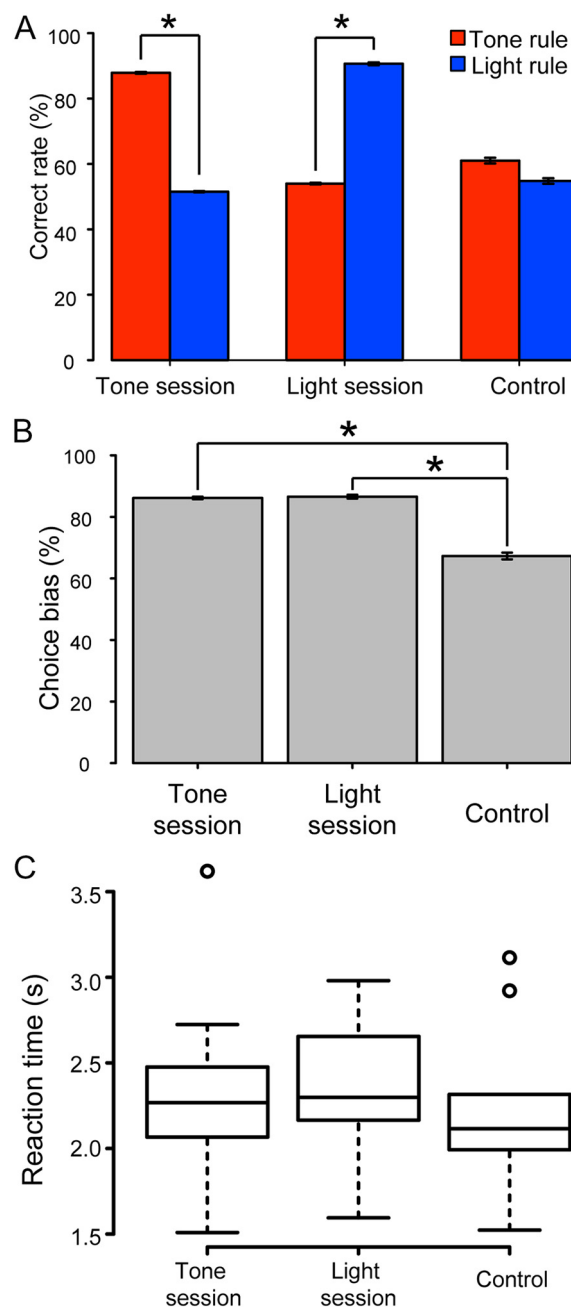
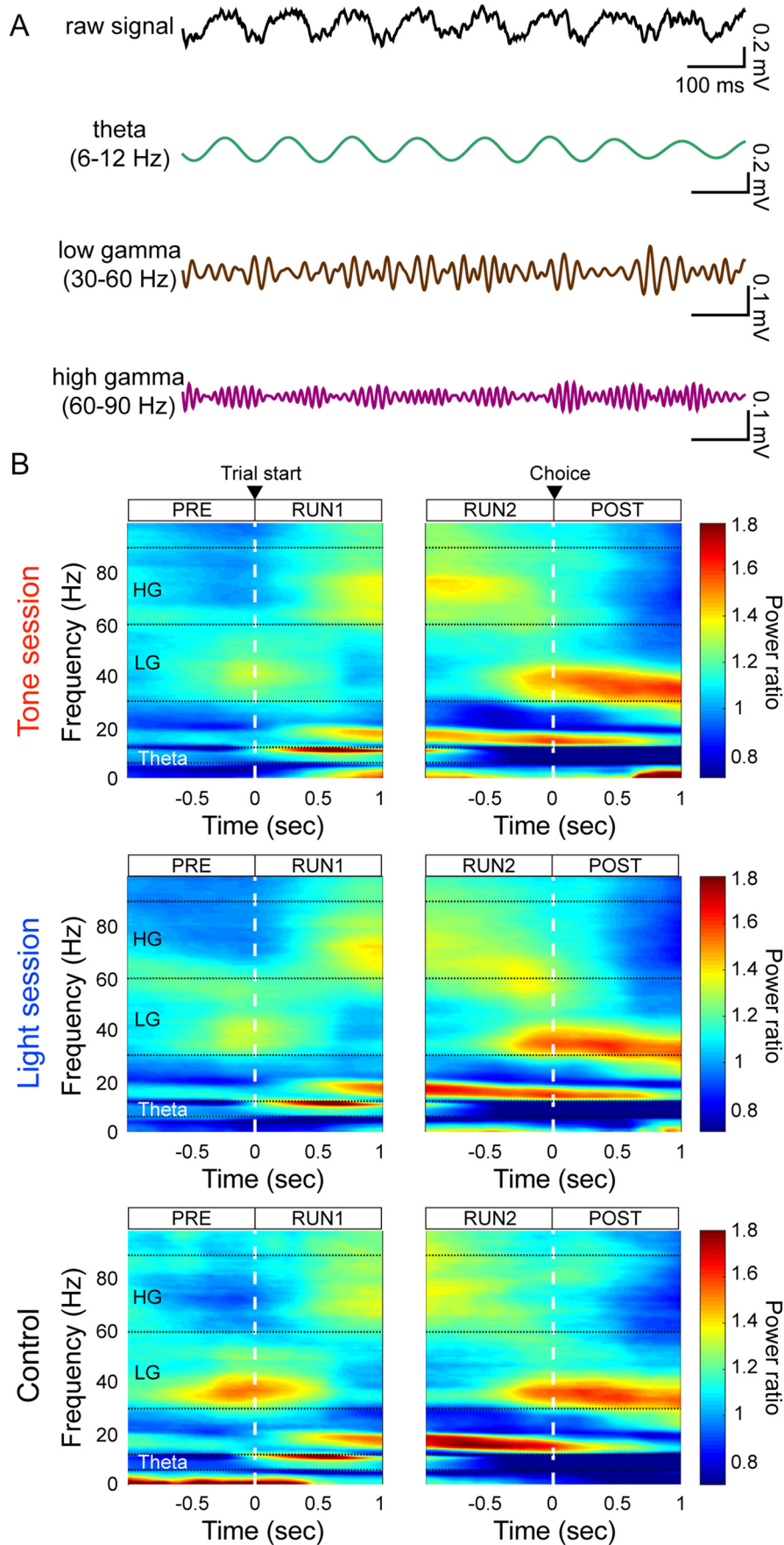


**Fig. 4. Behavioral performance during overtraining sessions**(A) Mean correct rates for both rules for each condition. Red bars show the mean correct rates for the tone rule, and blue bars show the mean correct rates for the light rule. (B) Mean choice bias. (C) Boxplot of reaction times for each condition. Lines inside the box represent medians. The bottom and top of the box show the first and third quartiles, respectively. Whiskers extend to the most extreme data point that is no more than 1.5 times the interquartile range from the box. Open circles show the values of data points that lie beyond the whiskers. Error bars in A and B show the standard error of the mean. Asterisks indicate significant differences of  $p < 0.05$ . (For interpretation of the references to color in this figure legend, the reader is referred to the web version of this article.)

6

Tomoaki Nakazono et al. / Neuroscience xxx (xxxx) xxx-xxx



## Evaluation of phase-amplitude coupling

To visualize the phase-amplitude coupling between theta and gamma oscillations, we calculated the frequency plot of the mean normalized power for the theta phase (Takahashi et al., 2014). These plots were based on the previously reported theta trough time-locked plots (Canolty et al., 2006; Tort et al., 2008), and drawn based on the theta phase angle. In addition, we constructed a histogram of the number of gamma peaks with 18° bins (Tort et al., 2008; Takahashi et al., 2014). Hilbert transformation of the filtered LFPs was performed, and the peak of gamma power was detected. This peak detection was performed within two consecutive theta cycles to prevent counting small peaks.

To quantify the intensity of phase-amplitude coupling between two frequency bands of interest (phase frequency and amplitude frequency), a modulation index (MI) was calculated and comodulograms were plotted (Canolty et al., 2006; Tort et al., 2008, 2009). The MI based on a normalized entropy measure is considered a suitable way to assess coupling intensity (Tort et al., 2010). First, the raw LFP signals were filtered at the phase frequency band and amplitude frequency band, respectively. Next, Hilbert transformation was performed, and the phase time series and amplitude time series were calculated. Then, the amplitude distribution over phase bins was constructed, and the divergence of the observed amplitude distribution from the uniform distribution was measured as the MI (Tort et al., 2008, 2009, 2010). A comodulogram is the color plot which shows MIs between frequency bands of the horizontal axis and amplitude band of the vertical axis. To plot the comodulograms, 4 and 10 Hz bins were used for frequency bands and amplitude frequency, respectively, and plotted MIs for these frequency windows as color maps.

For calculations, 20 Hz bandwidth data in each high and low gamma band with the most prominent coupling with theta oscillation for each rat were selected. First, the raw MI ( $M_{\text{raw}}$ ) was calculated. Next, the raw MIs were normalized using 200 surrogate data with shuffled phase and amplitude values within the trials (Kajihara et al., 2015) according to the following formula:

$$M_{\text{norm}} = \frac{(M_{\text{raw}} - \mu_{\text{surrogate}})}{\sigma_{\text{surrogate}}}$$

where  $\mu_{\text{surrogate}}$  denotes a mean of MIs from 200 surrogate data and  $\sigma_{\text{surrogate}}$  denotes the standard deviation of surrogate data. To examine the change in MIs during trial events or the learning process, the  $M_{\text{norm}}$  values were z-transformed for each rat to normalize individual differences. Statistical significance of coupling was assessed with a z-test using surrogate data.

## Assessment of learning effects

To investigate the effect of learning, we divided the learning process into two stages (i.e., early and late stages), distinguished by the point at which the correct rate for the new rule exceeded that for the previous rule. To detect the reversal point, we estimated the learning curves for both, new and previous rules (Smith et al., 2004). To assess learning effects on theta–gamma couplings, we divided each session into blocks consisting of 30 trials to ensure that MIs could be calculated (30 trials × 1 s for each event). The remaining trials were excluded from this analysis. To assess the relationship between the learning process and LFP data, we performed a regression analysis between the correct rates of non-match trials and LFP data.

## Statistical analysis

For analysis of behavioral data, paired *t*-test was performed for correct rate, one-way ANOVA for choice bias, and Kruskal–Wallis test for reaction times. A non-parametric test was used to compare reaction time data because the distribution of reaction time data does not follow a normal distribution. Two-factor repeated measures ANOVA was used to compare powers of LFPs and MIs. Tukey's HSD test was performed as post hoc analysis. To statistically examine the relationships between MIs and behavioral data, regression analysis was performed. Before parametric statistical tests were performed, normality of distributions and equal variances were confirmed using Kolmogorov–Smirnov test and Bartlett test respectively. Statistical analyses were performed using R (R version 3.0.1; The R Project for Statistical Computing).

## Histology

After the experiment was completed, rats were deeply anesthetized with an overdose of sodium pentobarbital (120 mg/kg) before the brains were perfused with a 10% buffered formalin solution. Following fixation, the brain was sectioned at a thickness of 50 μm. The locations of the electrode tips and cannula tracts in the brain was identified using a stereotaxic atlas (Paxinos and Watson, 2009).

## RESULTS

### Rats can learn the rule switching task

All animals performed the task for both, the tone and light rules. To examine the behavioral differences between these rules, we compared the performances during the overtraining sessions (i.e., a session after reaching the criteria for the tone rule and light rule) (Fig. 4). We calculated the correct rates for both, tone and light rules, from each overtraining session (Fig.

**Fig. 5. Changes in LFP power during trial events** (A) Example of LFP traces during the RUN2 event. The black line is the raw LFP. The green, brown, and purple lines represent the filtered LFP for theta, low-frequency gamma, and high-frequency gamma bands, respectively. (B) The mean power spectrograms for each condition (upper panels: tone session, middle panels: light session, lower panels: control session). Data from each animal were normalized using the mean power during the ITI and then averaged. Left panels show data for the 2 s surrounding the trial start ( $\pm 1$  s), and right panels show data for the 2 s surrounding the choice ( $\pm 1$  s). The vertical dashed white line denotes the center zero. The horizontal solid dotted black lines indicate borders of each frequency bands. HG and LG denote high-frequency gamma band and low-frequency gamma band, respectively. Error bars represent the standard error of the mean. (For interpretation of the references to color in this figure legend, the reader is referred to the web version of this article.)

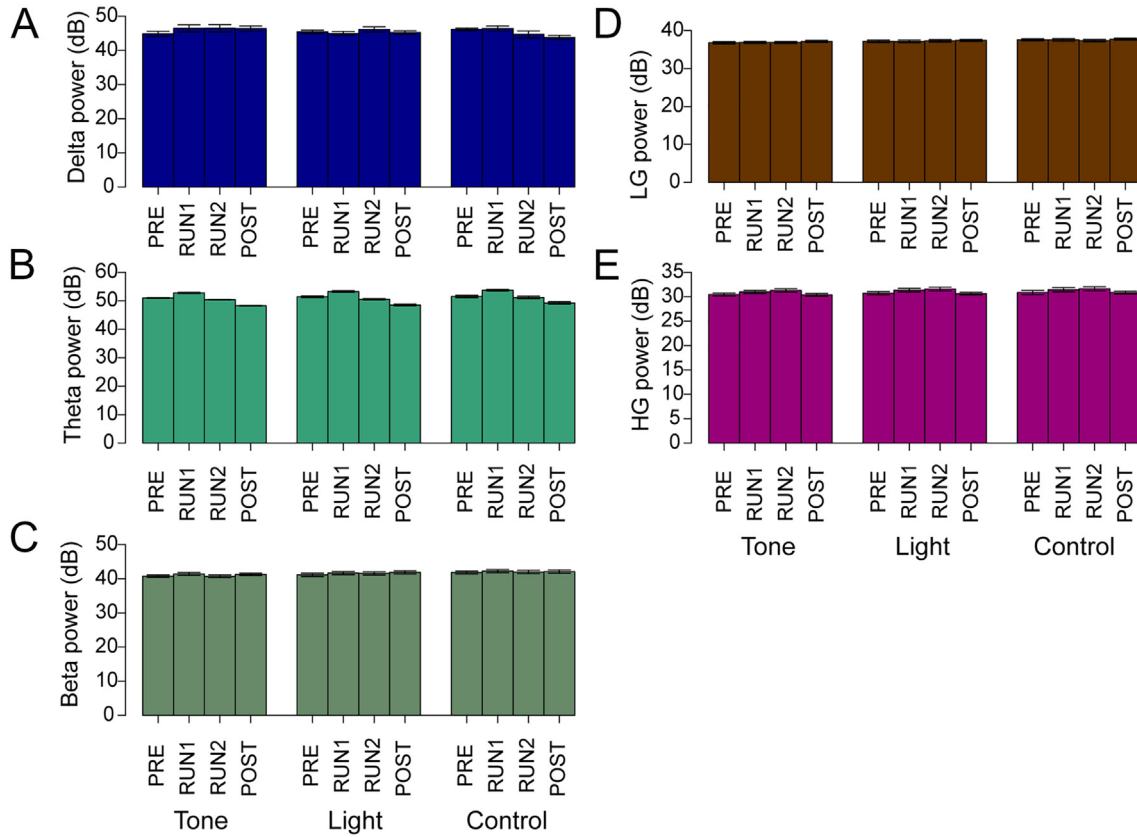


**Fig. 6. Comparison in LFP power of trial events** Mean power of delta (A), theta (B), beta (C), low-frequency gamma (D), and high-frequency gamma (E) for each condition (left: tone session, middle: light session, right: control session) and event. Error bars represent the standard error of the mean.

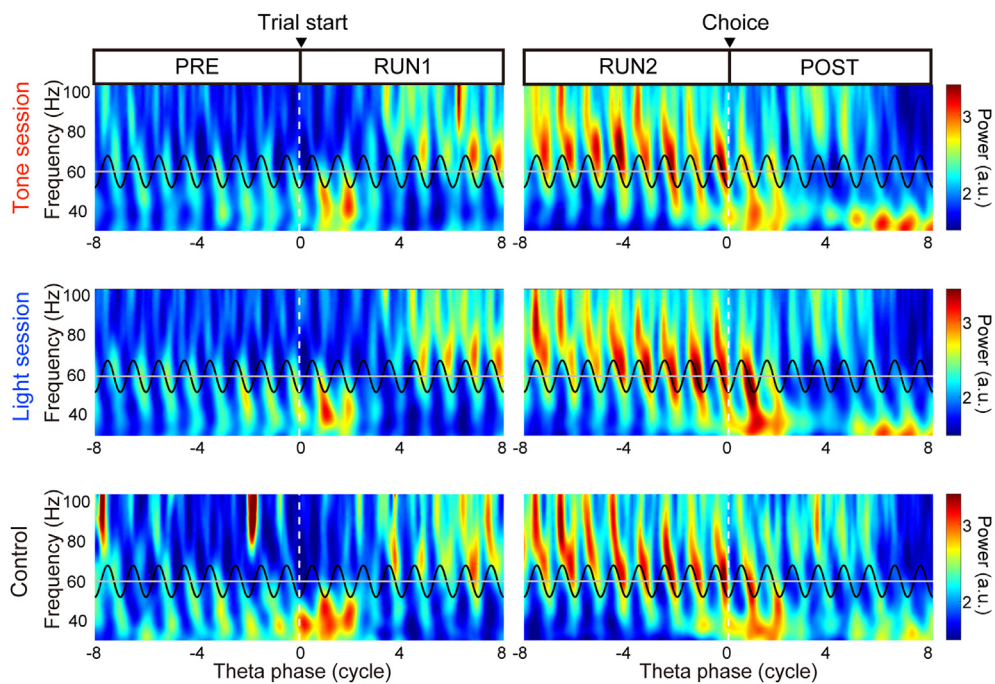


**Fig. 7. Theta modulation of gamma oscillations** Frequency plots of the mean normalized power for the theta phase for each condition (upper: tone session, middle: light session, lower: control). Data for ±8 cycles (nearly ±1 s) from the theta trough nearest to the trial start (left) and choice (right). The black solid line shows the theta phase. The vertical dashed white line denotes the center zero. The horizontal solid gray line shows the border between two gamma bands (60 Hz).

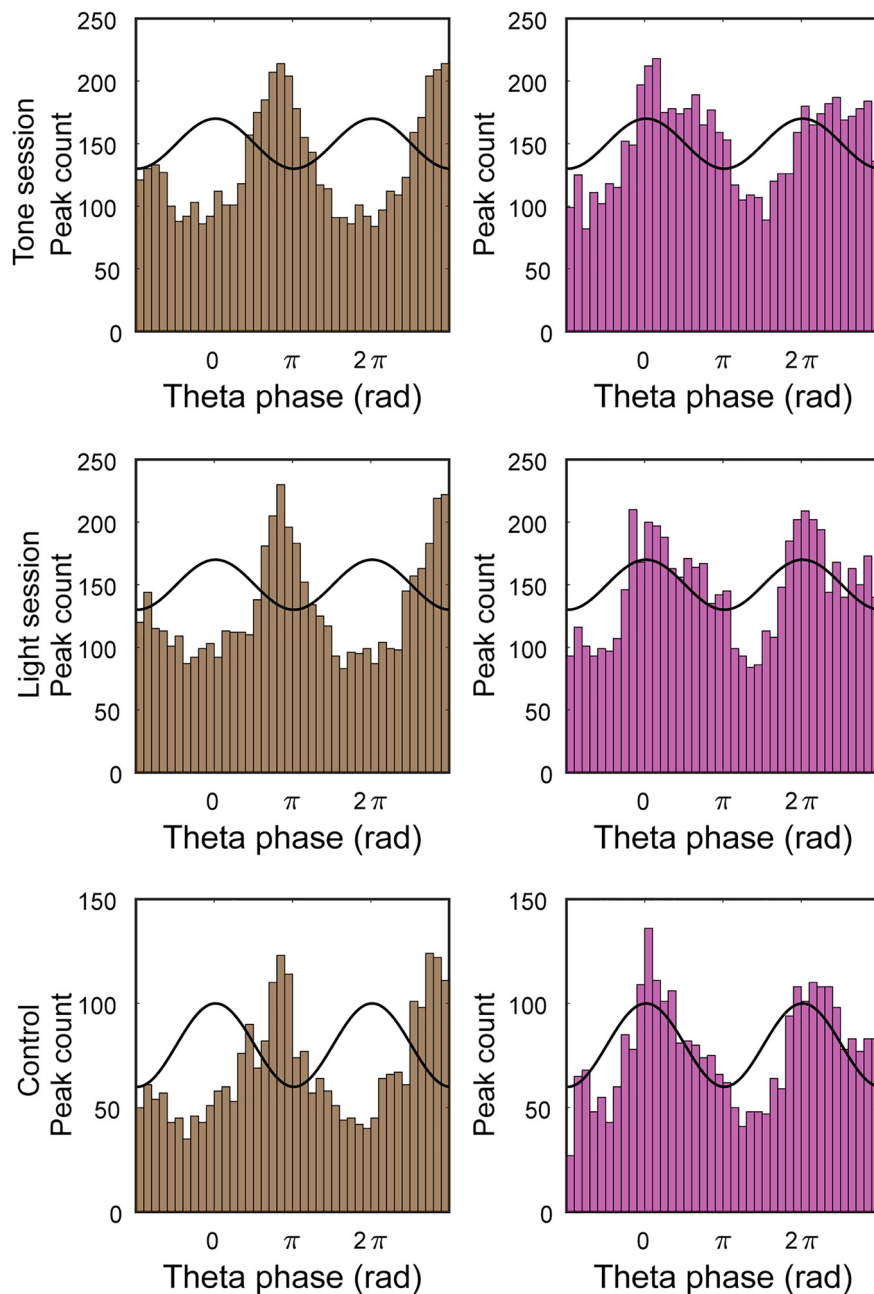


**Fig. 8. Histograms showing the number of gamma peaks in each theta phase** Left column (Brown bars): low-frequency gamma, right column (purple bars): high-frequency gamma. The black line shows the theta phase. The bin width is  $18^\circ$ . (For interpretation of the references to color in this figure legend, the reader is referred to the web version of this article.)

4A). To calculate the correct rates in the control sessions, we used data from the last sessions. For tone and light sessions, the correct rates for the new rule were significantly higher than the previous rule (paired  $t$ -test, tone session:  $t_{(13)} = -15.4461$ ,  $p < 0.001$ , light session:  $t_{(20)} = 20.0644$ ,  $p < 0.001$ ). However, the difference in the control session was not significant ( $t_{(9)} = 1.7056$ ,  $p = 0.1223$ , *n.s.*). To compare choice tendencies among the experimental conditions, we calculated choice bias. There were significant differences in choice bias among the conditions (Fig. 4B; one-way ANOVA,  $F_{(2, 42)} = 17.18$ ,  $p < 0.001$ ). The post hoc analysis (Tukey's HSD test) showed significant differences between the tone session vs. control session ( $p < 0.001$ ) and light

session vs. control session ( $p < 0.001$ ). However, there was no significant difference in reaction times (Fig. 4C; Kruskal-Wallis test,  $p = 0.4261$ , *n.s.*). These results show that rats understood the switching of the rules using trial and error learning, and used the correct rule during the overtraining session, but they did not show a rule preference during control sessions.

#### Effect of trial events and rules on LFP power

To assess the effect of trial events and rules on the LFP power, we recorded LFPs from the hippocampal CA1 area during an overtraining session and calculated the normalized

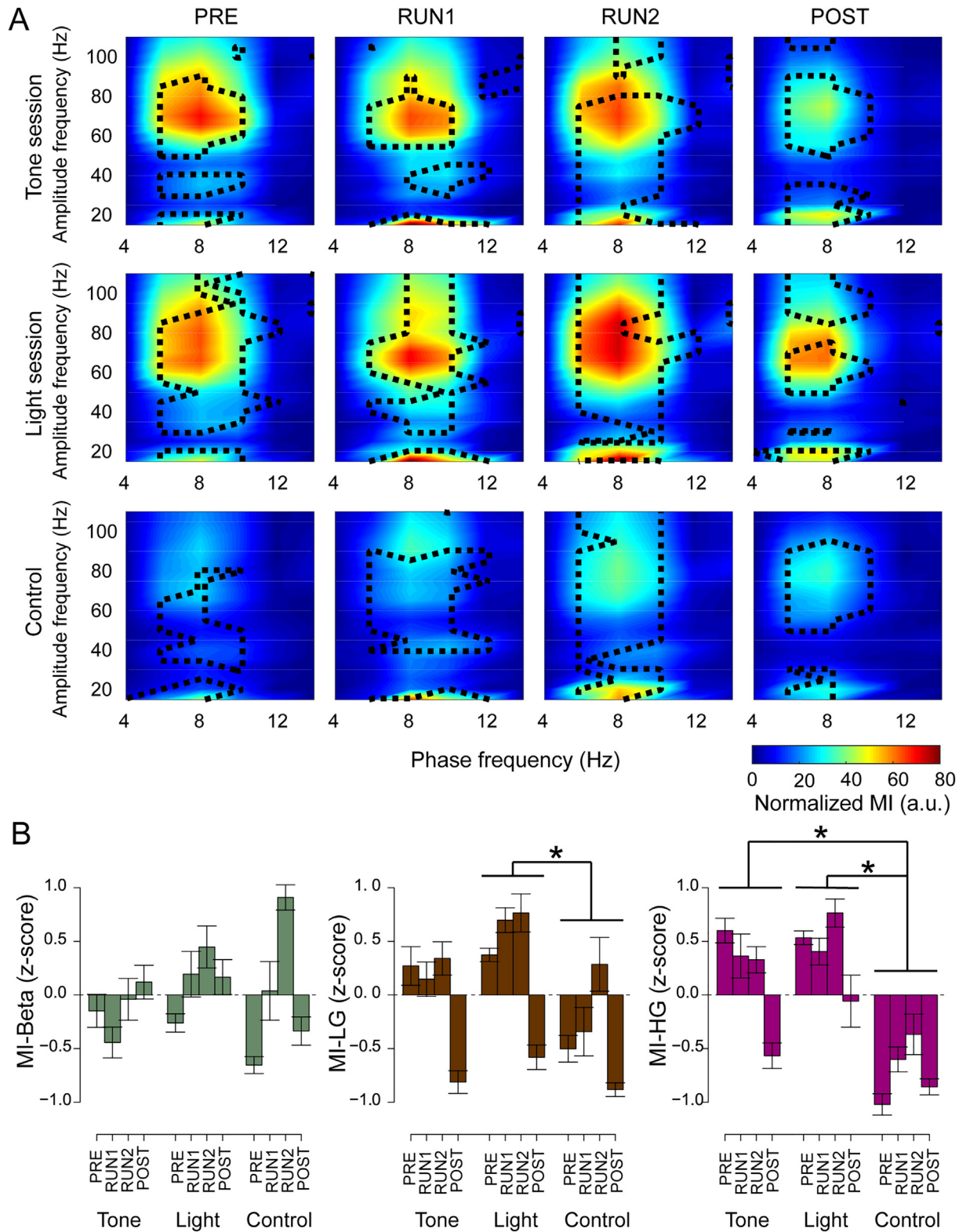


**Fig. 9. Phase-amplitude coupling during overtraining sessions**(A) Mean phase-amplitude comodulograms for each condition and event (upper: tone session, middle: light session, lower: control). The color map shows the MIs between phase frequency of the horizontal axis and amplitude frequency of the vertical axis. Data recorded from six rats were used to calculate the comodulograms and averaged to plot comodulograms. Areas enclosed by dotted black lines show significant couplings for all subjects. (B) Mean normalized modulation index between theta and beta (left), theta and low-frequency gamma (middle), and theta and high-frequency gamma (right), for each condition and event. Error bars represent the standard error of the mean. Asterisks indicate significant differences of  $p < 0.05$ .

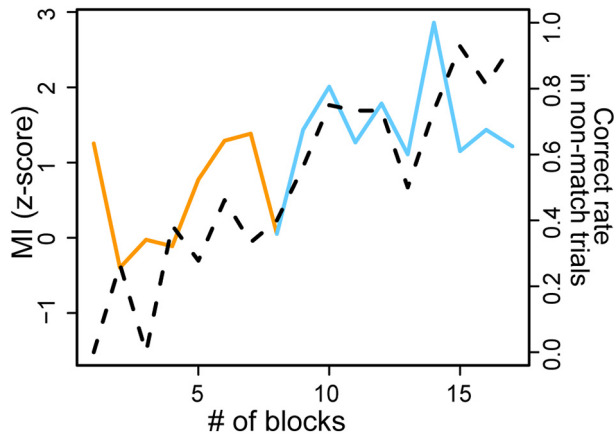


**Fig. 10. Example of change of theta–gamma coupling through rule learning** An example of the change in coupling strength between theta and high-frequency gamma. The colored solid line shows normalized MIs as a function of learning blocks. The orange part of the solid line shows the early learning stage, and the pale blue part shows the late learning stage. The black dashed line shows the correct rate for non-match trials per block. (For interpretation of the references to color in this figure legend, the reader is referred to the web version of this article.)

spectrograms for each condition to investigate changes in LFP power during the trials. Filtered LFP traces show prominent activities of theta, low gamma, and high gamma bands (Fig. 5A). To investigate LFP dynamics within a trial, we used four events (PRE, RUN1, RUN2, and POST). Because the median of reaction time was approximately 2 s (Fig. 4C), we considered the “RUN1” event as the former part and “RUN2” as the latter part of the period for choice selection. Fig. 5B shows that a prominent gamma band switched during the trial events. Low-frequency gamma power was prominent before the trial start (PRE) and after choice selection (POST),

whereas high-frequency gamma power was strong during choice selection (RUN1 and RUN2). To examine if there was significant change of LFP power between rules or task events, we performed a two-factor repeated measures ANOVA for each frequency bands. The results revealed no significant difference among conditions and events in delta power (1–4 Hz) and low-frequency gamma power (Fig. 6). However, theta power ( $F_{(3, 42)} = 127.384, p < 0.001$ ), beta power (15–30 Hz) ( $F_{(3, 42)} = 4.507, p < 0.01$ ), and high-gamma power ( $F_{(3, 42)} = 8.32, p < 0.001$ ) showed significant changes during the events but not in conditions. For the event effects in theta power, post hoc analysis (Tukey’s HSD test) revealed significant differences in all combinations of events except for PRE vs. RUN2. This suggested that theta power became prominent during choice running, especially in RUN1. For the event effects in high-gamma power, post hoc analysis revealed significant differences in PRE vs. RUN1, PRE vs. RUN2, RUN1 vs. POST, and RUN2 vs. POST. This suggested that changes in high-gamma power had similar tendencies to changes of theta power. In post hoc analysis of beta power, no significant difference between events was detected.

To examine the possibility that the power of LFPs was affected by sensory inputs, we also compared the power of each band among the four stimulus combinations using a two-factor repeated-measure ANOVA. Only one case (RUN2 event of light rule session) showed a significant difference in power of high-gamma power, suggesting that there was no consistent effect of sensory input on LFP power.

### Effect of trial events and rules on theta–gamma coupling

We investigated the presence of theta and gamma band coupling during the overtraining sessions. To visualize periodic

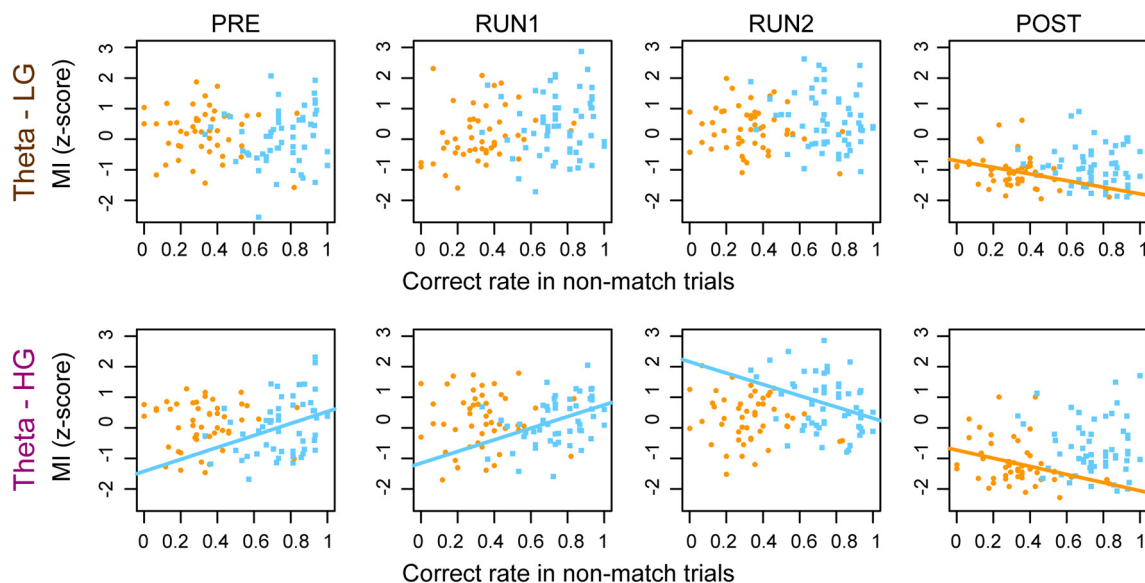


**Fig. 11. Relationships between theta–gamma coupling and correct rates** Scatter plots of normalized MIs vs. the correct rates in non-match trials for conditions and events. The upper panels show data for the coupling between theta and low-frequency gamma, and the lower panels show data for the coupling between theta and high-frequency gamma. The orange dots represent data from early stage blocks, and pale blue squares represent data from late stage blocks. Regression lines were plotted for significant relationships (orange: early stage, pale blue: late stage). (For interpretation of the references to color in this figure legend, the reader is referred to the web version of this article.)

modulations between theta and gamma, we calculated a frequency plot of the mean normalized power for the theta phase of each condition (Fig. 7). In Fig. 7, both low-frequency and high-frequency gamma bands show a stripe-like pattern similar to a theta rhythm. This pattern suggests that gamma power was modulated by the theta rhythms. Furthermore, Fig. 8 shows that the amplitude of high-frequency gamma became prominent around the descending theta phase, and that of low-frequency gamma became prominent around the negative trough of the theta cycle. This result confirms that high-frequency and low-frequency gamma bands show distinct coupling patterns with theta oscillations.

Next, we calculated the CFC using the MI and plotted comodulograms to quantify the theta–gamma coupling for each condition. These comodulograms show that the theta phase strongly modulated the gamma amplitude in all the conditions (Fig. 9A). The coupling between theta and high-frequency gamma appeared stronger than the coupling between theta and low-frequency gamma; however, the theta and low-frequency gamma coupling also showed statistical significance in most cases. In addition, the coupling for the control condition appeared weaker than the experimental conditions as shown in Fig. 9A. To quantify this difference, we compared the MIs among the conditions and events using a two-factor factorial ANOVA (Fig. 9B). For the coupling between theta and low-frequency gamma, the effects of condition ( $F_{(2, 56)} = 3.361, p < 0.05$ ) and event ( $F_{(3, 56)} = 6.407, p < 0.001$ ) were significant. For the condition effects, a post hoc analysis (Tukey's HSD test) revealed a significant difference between the light conditions vs. the control condition ( $p < 0.05$ ). For the event effects, the MI for POST was significantly weaker than the other three events (PRE vs. POST:  $p < 0.05$ , RUN1 vs. POST:  $p < 0.05$ , RUN2 vs. POST:  $p < 0.001$ ). For the coupling between theta and high-frequency gamma, the effect of condition was significant ( $F_{(2, 56)} = 10.793, p < 0.001$ ), but the effect of events was not ( $F_{(3, 56)} = 2.604, p = 0.06, n.s.$ ). For the condition effects, post hoc analysis showed significant differences between the light condition vs. the control condition ( $p < 0.001$ ) and between the tone conditions vs. the control condition ( $p < 0.01$ ). These results show that theta–gamma coupling was modulated by rule-guided behavior. MIs between theta and beta oscillation were also compared. However, neither event nor condition effects showed significant differences. As the coupling between theta and beta oscillations did not show significant changes between conditions, this coupling was excluded from subsequent analyses.

### Effect of learning a new rule on theta–gamma coupling

We investigated the effect of rule learning on both theta and low-frequency gamma coupling and theta and high-frequency gamma coupling. In this analysis, we only used data from the first rule switching process (tone rule to light rule) because the LFP signals tended to become unstable after a second rule switch process. In the first switching

process, animals already understood the tone rule, whereas the light rule was novel. Fig. 2 shows an example of learning process. The learning process was separated into two stages (early and late). The mean number of trials for the early stage was 298.67 (SD = 162.4), and the mean number of trials until the completion of learning was 681.67 (SD = 261.88). Fig. 10 shows an example of the change in MIs of theta and high-frequency gamma coupling during the RUN1 event. This example shows that theta–gamma coupling increased with the learning process, as previously reported (Tort et al., 2008, 2009; Lopes-dos-Santos et al., 2018). To statistically examine these relationships, we performed a regression analysis of normalized MIs vs. the correct rate for each event (Fig. 11). Fig. 11 shows different tendencies between theta and low-frequency gamma coupling and theta and high-frequency gamma coupling. For theta and low-frequency gamma coupling, the coupling during POST became weaker during the early learning stage. In contrast, theta and high-frequency gamma coupling showed learning stage-dependent dynamics. Coupling during POST became weaker during the early stage as with low gamma. During the late stage, coupling strengths during PRE and RUN1 became stronger, whereas the coupling during RUN2 became weaker. We also investigated the effect of match trials vs non-match trials on the theta–gamma coupling; however, no relationship was found between the trial types and changes in coupling intensity.

To investigate the relationship between correct rate and reaction time, and the relationships between the correct rate and LFP power, regression analysis was performed (Fig. 12). For this analysis, LFP data from events in which each LFP band showed the most prominent power (theta: RUN1, low gamma: POST, high gamma: RUN2) were used. Fig. 12 shows that there were no significant relationships between reaction time and learning, or between learning and LFP powers.

## DISCUSSION

In this study, we designed a novel rule-switching task with a control condition, and recorded LFPs from the hippocampal CA1. Our results showed that the strength of cross frequency coupling between theta and gamma oscillations was stronger in rule-guided behavior than that in the no rule condition. The results also confirmed previous studies that have reported an enhancement of theta–gamma coupling in the rodent hippocampus during learning (Tort et al., 2008, 2009; Lopes-dos-Santos et al., 2018). In addition, coupling between theta and high-frequency gamma showed characteristic dynamics during the late stage of learning.

As it is known that spikes can contaminate high frequency oscillations of LFPs, caution must be exercised when discussing activities of these oscillations. Belluscio et al. (2012) reported that spikes can affect oscillations above 100 Hz in the hippocampus. As we analyzed oscillations under 90 Hz, we considered that the effects of spike contamination were not critical for our results.

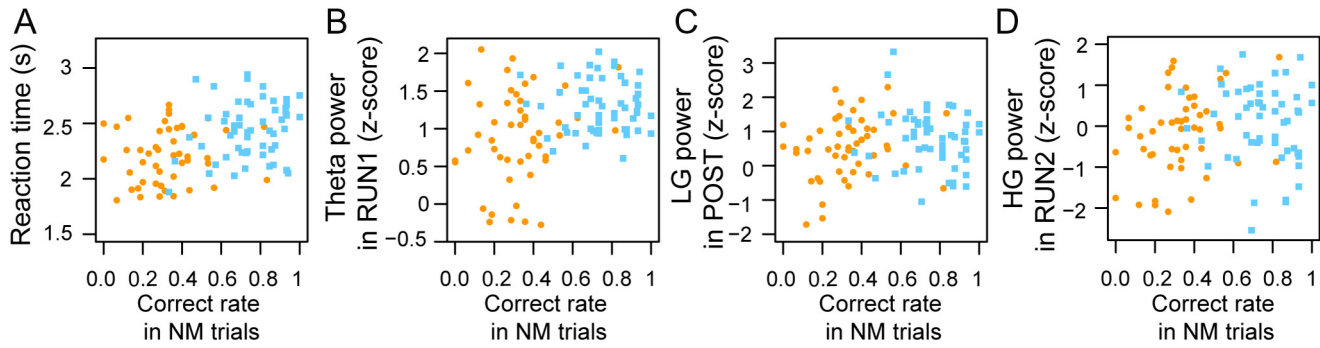


**Fig. 12. Relationships between correct rate and other indices** Scatter plot of reaction times (A), theta power (B), low frequency gamma power (C), and high frequency gamma power (D) vs. the correct rate in non-match trials. The orange dots represent data from early stage blocks, and pale blue squares represent data from late stage blocks. (For interpretation of the references to color in this figure legend, the reader is referred to the web version of this article.)

## Rats learned rules by trial and error

Fig. 4A and B shows that the animals learned to use the correct rule during experimental conditions; however, they did not use any specific rule during the control condition. In addition, there was no significant difference in reaction times between the conditions (Fig. 4C). These results suggest that even if the motor output, reward, and sensory inputs were similar under both the conditions, animals did not have any behavioral rules during the control condition.

## Theta–gamma coupling in the hippocampus is involved in the processing of rules

Besides the involvement in spatial information processing (O'Keefe and Dostrovsky, 1971), previous studies have revealed that the hippocampus is involved in various types of non-spatial and abstract information processing, such as context (Wood et al., 2000; Takahashi, 2013), working memory (Sakurai, 1994; Deadwyler et al., 1996; Takahashi and Sakurai, 2009), and temporal information (MacDonald et al., 2011; Nakazono et al., 2015). In addition to those previous studies, our study showed that the theta–gamma coupling in the hippocampus is involved in the processing of abstract information (i.e., rules).

In general, rule learning is thought to be processed by the prefrontal cortex (Hoshi et al., 2000; Rich and Shapiro, 2009; Durstewitz et al., 2010). However, it was reported that the interaction between the prefrontal cortex and hippocampus also plays an important role in this type of learning (Peyrache et al., 2009; Benchenane et al., 2010). Furthermore, hippocampal neurons change their activity when the rule or strategy changes (Smith and Mizumori, 2006; Gill et al., 2011; Takahashi, 2013). A pharmacological inactivation study also reported that the dorsal hippocampus is necessary for the learning of declarative-like memories of the relationship between non-spatial cues and reward (Jacquet et al., 2013). Considering these previous reports, it is plausible that the hippocampus is involved in even non-spatial task learning. Indeed, previous studies have already shown that the strength of theta–gamma coupling became stronger through learning that the CFC in the hippocampus contributes to rule learning (Tort et al., 2008, 2009; Lopes-dos-Santos et al., 2018). However, the effect of reward magnitude was not considered and might be a confounding factor in these previous studies.

To exclude this possibility and to answer our first question, we compared the LFPs between rule-guided conditions and the control condition. As the control condition had the same sensory stimulus as that in experimental conditions and rats made their decision regardless of stimulus in the control condition (Fig. 4B), we considered that this control condition could disentangle the effect of knowledge of rules from sensory input and other factors. The LFP power did not significantly change based on the condition (Fig. 6). However, the strength of theta–gamma coupling was weaker in control condition than the experimental conditions (Fig. 9). Because sensory inputs, motor outputs, and the amount of reward were similar across the conditions, and rats made their decisions independently of

presented stimuli (Fig. 4B), it is likely that the strength of theta–gamma coupling reflected knowledge of the rule (task demand). These results rule out the possibility that enhancement of theta–gamma coupling was caused by an increase in the amount of reward.

In contrast, theta–beta couplings did not show task-related changes (Fig. 9B); nevertheless, the power of beta oscillation showed significant changes through task events (Fig. 6C). These results suggested that beta and gamma oscillations have different functions and underlying mechanisms. A previous study on beta oscillation suggested that beta oscillation is a prominent rhythm in the olfactory pathway and may reflect top-down signals through this pathway (Martin and Ravel, 2014). Another study reported task-related beta oscillations in hippocampal CA1 of rats performing an odor reward association task (Rangel et al., 2016). Therefore, it is plausible that beta oscillations did not play an important role in our task because it was not an odor-dependent task.

## Differential dynamics in gamma oscillations during learning

Previous studies have reported that there are functional differences between low and high-frequency gamma bands (Colgin et al., 2009; Bieri et al., 2014; Zheng et al., 2015a). Furthermore, a recent study suggested that there were also functional differences in the gamma types in coupling with theta during the learning of a spatial task (Lopes-dos-Santos et al., 2018). Our results also showed differences in the effects of learning on low and high-frequency gamma bands (Fig. 11). In the early learning stage, both low and high-frequency gamma decreased coupling strength with theta. Because this decrease occurred during the 1 s after choice (POST) when animals could determine the result of their choice, there is a possibility that these changes were related to prediction error. Just after rule switching, animals may predict reward even in error trials for the new rule and show prediction error. However, such prediction errors would disappear as learning progressed.

On the other hand, changes in theta–gamma coupling in the late learning stage were more complex. During the  $\pm 1$  s from trial start (PRE and RUN1), the strength of theta–high gamma coupling increased as the learning progressed. In contrast, it became weak during the 1 s before choice (RUN2). The increase in theta and high gamma coupling strength through learning is in agreement with the results of previous studies (Tort et al., 2008; Lopes-dos-Santos et al., 2018). Notably, changes in theta–high gamma coupling during the former and latter parts of choice run (RUN1 and RUN2) showed opposing tendencies. Amemiya and Redish (2018) suggested that the high gamma dominant theta cycle appears when animals approach a choice point in a spatial decision-making task. Our results were inconsistent with this previous report. However, this discrepancy may be explained by the difference in behavioral tasks. In our task, cues were presented just after the trial start. Therefore, it is possible that the timing of decision making was shifted from near choice (RUN2) to trial-start (RUN1) because the animals were able

to make decisions faster as learning progressed. It may also be possible that changes in spatial information of decision making caused changes in theta–high gamma coupling. As we were unable to determine where the rats performed decision making in this task, we could not exclude this possibility. However, there was no difference in power of LFP and CFC between right and left hole choices; thus, the effect of spatial information on changes in theta–gamma coupling are likely to be limited.

With regard to our second and third questions, our data suggested that theta–gamma coupling in the hippocampus was not involved in the trial and error process. Instead, it was involved in the process of knowledge acquisition. Furthermore, only theta–high gamma coupling showed correlated changes with learning.

However, it remains unclear if changes in theta–gamma coupling were affected by other factors. There are two possible factors, running speed and powers of LFPs, which may affect theta–gamma coupling (Tort et al., 2009; Sheremet et al., 2019). Tort et al. (2009) reported that MI calculation can be affected by LFP powers. Because running speed can alter theta power (Montgomery et al., 2009) and gamma power (Ahmed and Mehta, 2012), especially high-gamma power (Zheng et al., 2015b), it is plausible that changes in running speed may affect both LFP power and theta–gamma coupling. As shown in Fig. 6, significant changes in theta power and high-gamma power were detected through events, and these powers became stronger during running. However, comparison of reaction times between conditions showed no significant changes (Fig. 4C), and reaction times did not change through learning (Fig. 12A). Therefore, the changes in theta–gamma coupling by events and learning are unlikely to be due to changes in reaction times. Nevertheless, the possibility remains that changes in LFP power affected the coupling regardless of reaction times. This hypothesis is plausible because both theta power and gamma power can be altered by cognitive state (Montgomery and Buzsáki, 2007; Nakazono et al., 2015). However, as shown in Fig. 12B–D, there was no significant relationship between LFP powers and learning. These results suggested that neither changes in reaction time nor changes in LFP power could explain changes in theta–gamma couplings in our task.

### What role does theta–gamma coupling have in rule-switching learning?

As Fig. 8 shows, high-frequency gamma and low-frequency gamma were coupled with different phases of theta. This phenomenon is thought to reflect the switching of information processing in the hippocampus by the theta phase (Hasselmo, 2005; Mizuseki et al., 2009; Schomburg et al., 2014). It is considered that the high-frequency gamma reflects information flow from the entorhinal cortex to CA1, whereas low-frequency gamma reflects information flow from the CA3 region (Colgin et al., 2009). In spatial information coding, high-frequency gamma and low-frequency gamma are thought to be related to “retrospective coding” and “prospective coding”, respectively (Bieri et al., 2014; Takahashi et al., 2014). Retrospective coding is used to encode sensory

or spatial information in the past, and prospective coding is to recall information in future behavior.

As we hypothesized, our data showed that there were different effects on high-frequency gamma and low-frequency gamma coupling with theta during learning. The results on the increase in strength of theta–high gamma coupling through learning are consistent with previous reports (Tort et al., 2008; Lopes-dos-Santos et al., 2018). Our results also revealed that such enhancement occurred not during trial and error challenge, but when the animals acquired new knowledge. Our data also suggested that theta and low-frequency gamma coupling did not have important roles in the learning of this task.

The hippocampal CA1 region is thought to participate in cognitive tasks as a part of a neuronal circuit, composed of the PFC, OFC, thalamic nucleus reuniens (NR), and medial entorhinal cortex (MEC) (Benchenane et al., 2010; Yamamoto et al., 2014; Ito et al., 2015). A previous study (Yamamoto et al., 2014) suggested that the PFC and OFC send information about rules to both the hippocampal CA1 and MEC via the NR, and this projection drives the CA1-MEC circuit to process task-related sensory information. We speculate that the changes in theta and high-frequency gamma coupling during learning reflect changes in activity of this circuit. During the early stage of learning when rats continued the task with trial and error, they did not have reliable information on rules, and the PFC/OFC-CA1/MEC circuit was not involved. However, after rats started learning the new rule, this neural circuit was engaged. We speculate that the PFC and OFC send information about rules to the hippocampus and MEC, which drive CA1-MEC circuits to process sensory inputs more effectively. The coupling between theta and high-frequency gamma became stronger because the CA1-MEC circuit became more active. This enhancement occurred during the late learning stage. In contrast, coupling just before choice became weaker because animals decided their actions just after stimulus onset during the late learning stage.

These results suggest the possibility that CFCs have rich information about non-spatial cognitive tasks and contribute to dynamic changes in cell assembly. Furthermore, these dynamics in the hippocampus are thought to reflect information flow from other brain areas. However, in this study, we did not elucidate causal relationships between theta–gamma coupling and dynamics of cell assembly. Future work is needed to reveal the relationships among CFC, types of oscillation, dynamic cell assembly, and the interactions among different brain areas.

### ACKNOWLEDGMENTS

This research was supported by Japan Society for the Promotion of Science (Nos. 16H01283, 16H02061, and 18H05088 to YS, Nos. 19H01131 and 16H06543 to ST, and No. 11J07301 and 19K16884 to TN), by Ministry of Internal Affairs and Communications (MIC SCOPE 152107008 to ST), and by the Sasakawa Scientific Research Grant from The Japan Science Society to TN. We thank Dr. Adriano Tort for providing the Matlab codes to calculate the modulation

index. We also thank Dr. Muneyoshi Takahashi and Dr. Hiroshi Nishida for their advice about the analysis.

### AUTHOR CONTRIBUTIONS

TN designed the research plan with advice by YS. TN performed the experiments and wrote the original manuscript. ST contributed to data analysis. All of the authors discussed the results and approved the manuscript.

### CONFLICT OF INTEREST

The authors declare that there is no conflict of interest regarding the publication of this paper.

### REFERENCES

- Ahmed OJ, Mehta MR. (2012) Running speed alters the frequency of hippocampal gamma oscillations. *J Neurosci* 32:7373–7383.
- Amemiyama S, Redish AD. (2018) Hippocampal theta–gamma coupling reflects state-dependent information processing in decision making. *Cell Rep* 22:3328–3338.
- Belluscio MA, Mizuseki K, Schmidt R, Kempter R, Buzsáki G. (2012) Cross-frequency phase–phase coupling between theta and gamma oscillations in the hippocampus. *J Neurosci* 32:423–435.
- Benchenane K, Peyrache A, Khamassi M, Tierney PL, Gioanni Y, Battaglia FP, Wiener SI. (2010) Coherent theta oscillations and reorganization of spike timing in the hippocampal–prefrontal network upon learning. *Neuron* 66:921–936.
- Bieri KW, Bobbitt KN, Colgin LL. (2014) Slow and fast gamma rhythms coordinate different spatial coding modes in hippocampal place cells. *Neuron* 82:670–681.
- Buzsáki G. (2010) Neural syntax: cell assemblies, synapsembles, and readers. *Neuron* 68:362–385.
- Canolty RT, Edwards E, Dalal SS, Soltani M, Nagarajan SS, Kirsch HE, Berger MS, Barbare NM, Knight RT. (2006) High gamma power is phase-locked to theta oscillations in human neocortex. *Science* 313:1626–1628.
- Canolty RT, Ganguly K, Kennerley SW, Cadieu CF, Koepsell K, Wallis JD, Carmena JM. (2010) Oscillatory phase coupling coordinates anatomically dispersed functional cell assemblies. *Proc Natl Acad Sci* 107:17356–17361.
- Colgin LL, Denninger T, Fyhn M, Hafting T, Bonnevie T, Jensen O, Moser M-B, Moser EI. (2009) Frequency of gamma oscillations routes flow of information in the hippocampus. *Nature* 462:353–357.
- Deadwyler SA, Hampson E, Forest W, Carolina N, Bunn T, Hampson RE. (1996) Hippocampal ensemble activity during spatial performance in rats. *J Neurosci* 16:354–372.
- Dragoi G, Buzsáki G. (2006) Temporal encoding of place sequences by hippocampal cell assemblies. *Neuron* 50:145–157.
- Durstewitz D, Vitoz NM, Floresco SB, Seamans JK. (2010) Abrupt transitions between prefrontal neural ensemble states accompany behavioral transitions during rule learning. *Neuron* 66:438–448.
- Fries P, Reynolds JH, Rorie AE, Desimone R. (2001) Modulation of oscillatory neuronal synchronization by selective visual attention. *Science* 291:1560–1563.
- Gill PR, Mizumori SJY, Smith DM. (2011) Hippocampal episode fields develop with learning. *Hippocampus* 21:1240–1249.
- Harris KD. (2005) Neural signatures of cell assembly organization. *Nat Rev Neurosci* 6:399–407.
- Harris KD, Csicsvari J, Hirase H, Dragoi G, Buzsáki G. (2003) Organization of cell assemblies in the hippocampus. *Nature* 424:552–556.
- Hasselmo ME. (2005) What is the function of hippocampal theta rhythm? Linking behavioral data to phasic properties of field potential and unit recording data. *Hippocampus* 15:936–949.
- Hebb DO. (1949) *The organization of behavior—a neuropsychological theory*. New York: Wiley, 1949.
- Hoshi E, Shima K, Tanji J. (2000) Neuronal activity in the primate prefrontal cortex in the process of motor selection based on two behavioral rules. *J Neurophysiol* 83:2355–2373.
- Igarashi J, Isomura Y, Arai K, Harukuni R, Fukai T. (2013) A theta–gamma oscillation code for neuronal coordination during motor behavior. *J Neurosci* 33:18515–18530.
- Ito HT, Zhang S-J, Witter MP, Moser EI, Moser M-B. (2015) A prefrontal–thalamo–hippocampal circuit for goal-directed spatial navigation. *Nature* 522:50–55.
- Jacquet M, Lecourtier L, Cassel R, Loureiro M, Cosquer B, Escoffier G, Migliorati M, Cassel JC, Roman FS, Marchetti E. (2013) Dorsolateral striatum and dorsal hippocampus: a serial contribution to acquisition of cue–reward associations in rats. *Behav Brain Res* 239:94–103.
- Kajihara T, Anwar MN, Kawasaki M, Mizuno Y, Nakazawa K, Kitajo K. (2015) Neural dynamics in motor preparation: from phase-mediated global computation to amplitude-mediated local computation. *Neuroimage* 118:445–455.
- Li S, Bai W, Liu T, Yi H, Tian X. (2012) Increases of theta–low gamma coupling in rat medial prefrontal cortex during working memory task. *Brain Res Bull* 89:115–123.
- Lisman JE, Jensen O. (2013) The theta–gamma neural code. *Neuron* 77:1002–1016.
- Lopes-dos-Santos V, van de Ven GM, Morley A, Trouche S, Campo-Urriza N, Dupret D. (2018) Parsing hippocampal theta oscillations by nested spectral components during spatial exploration and memory-guided behavior. *Neuron* 100:940–952.
- MacDonald CJ, Lepage KQ, Eden UT, Eichenbaum H. (2011) Hippocampal “time cells” bridge the gap in memory for discontinuous events. *Neuron* 71:737–749.
- Martin C, Ravel N. (2014) Beta and gamma oscillatory activities associated with olfactory memory tasks: different rhythms for different functional networks? *Front Behav Neurosci* 8:218.
- McNaughton BL, Barnes CA, Meltzer J, Sutherland RJ. (1989) Hippocampal granule cells are necessary for normal spatial learning but not for spatially-selective pyramidal cell discharge. *Exp Brain Res* 76:485–496.
- Mitra P, Bokil H. (2007) *Observed brain dynamics*. New York: Oxford University Press, 2007.
- Mizuhara H, Sato N, Yamaguchi Y. (2015) Cortical networks dynamically emerge with the interplay of slow and fast oscillations for memory of a natural scene. *Neuroimage* 111:76–84.
- Mizuseki K, Sirota A, Pastalkova E, Buzsáki G. (2009) Theta oscillations provide temporal windows for local circuit computation in the entorhinal–hippocampal loop. *Neuron* 64:267–280.
- Montgomery SM, Betancur MI, Buzsáki G. (2009) Behavior-dependent coordination of multiple theta dipoles in the hippocampus. *J Neurosci* 29:1381–1394.
- Montgomery SM, Buzsáki G. (2007) Gamma oscillations dynamically couple hippocampal CA3 and CA1 regions during memory task performance. *Proc Natl Acad Sci U S A* 104:14495–14500.
- Nakazono T, Sano T, Takahashi S, Sakurai Y. (2015) Theta oscillation and neuronal activity in rat hippocampus are involved in temporal discrimination of time in seconds. *Front Syst Neurosci* 9:1–12.
- Nishida H, Takahashi M, Lauwereyns J. (2014) Within-session dynamics of theta–gamma coupling and high-frequency oscillations during spatial alternation in rat hippocampal area CA1. *Cogn Neurodyn* 8:363–372.
- O’Keefe J, Dostrovsky J. (1971) The hippocampus as a spatial map. Preliminary evidence from unit activity in the freely-moving rat. *Brain Res* 34:171–175.
- Paxinos G, Watson C. (2009) *The rat brain in stereotaxic coordinates, compact Si*. New York: Academic Press, 2009.
- Peyrache A, Khamassi M, Benchenane K, Wiener SI, Battaglia FP. (2009) Replay of rule-learning related neural patterns in the prefrontal cortex during sleep. *Nat Neurosci* 12:919–926.
- Rangel LM, Rueckemann JW, Riviere PD, Keefe KR, Porter BS, Heimbuch IS, Budlong CH, Eichenbaum H. (2016) Rhythmic coordination

- of hippocampal neurons during associative memory processing. *eLife* 5:e09849.
- Rich EL, Shapiro M. (2009) Rat prefrontal cortical neurons selectively code strategy switches. *J Neurosci* 29:7208–7219.
- Sakata S, Kitsukawa T, Kaneko T, Yamamori T, Sakurai Y. (2002) Task-dependent and cell-type-specific Fos enhancement in rat sensory cortices during audio-visual discrimination. *Eur J Neurosci* 15:735–743.
- Sakurai Y. (1994) Involvement of auditory cortical and hippocampal neurons in auditory working memory and reference memory in the rat. *J Neurosci* 14:2606–2623.
- Sakurai Y. (1996) Hippocampal and neocortical cell assemblies encode memory processes for different types of stimuli in the rat. *J Neurosci* 16:2809–2819.
- Sakurai Y. (1999) How do cell assemblies encode information in the brain? *Neurosci Biobehav Rev* 23:785–796.
- Sakurai Y. (2002) Coding of auditory temporal and pitch information by hippocampal individual cells and cell assemblies in the rat. *Neuroscience* 115:1153–1163.
- Schomburg EW, Fernández-Ruiz A, Mizuseki K, Berényi A, Anastassiou CA, Koch C, Buzsáki G. (2014) Theta phase segregation of input-specific gamma patterns in entorhinal-hippocampal networks. *Neuron* 84:470–485.
- Sheremet A, Kennedy JP, Qin Y, Zhou Y, Lovett SD, Burke SN, Maurer AP. (2019) Theta–gamma cascades and running speed. *J Neurophysiol* 121:444–458.
- Shirvalkar PR, Rapp PR, Shapiro ML. (2010) Bidirectional changes to hippocampal theta–gamma comodulation predict memory for recent spatial episodes. *Proc Natl Acad Sci* 107:7054–7059.
- Smith AC, Frank LM, Wirth S, Yanike M, Hu D, Kubota Y, Graybiel AM, Suzuki WA, Brown EN. (2004) Dynamic analysis of learning in behavioral experiments. *J Neurosci* 24:447–461.
- Smith DM, Mizumori SJY. (2006) Hippocampal place cells, context, and episodic memory. *Hippocampus* 16:716–729.
- Takahashi M, Nishida H, Redish AD, Lauwereyns J. (2014) Theta phase shift in spike timing and modulation of gamma oscillation: a dynamic code for spatial alternation during fixation in rat hippocampal area CA1. *J Neurophysiol* 111:1601–1614.
- Takahashi S. (2013) Hierarchical organization of context in the hippocampal episodic code. *eLife* 2:e00321.
- Takahashi S, Anzai Y, Sakurai Y. (2003) Automatic sorting for multi-neuronal activity recorded with tetrodes in the presence of overlapping spikes. *J Neurophysiol* 89:2245–2258.
- Takahashi S, Anzai Y, Sakurai Y. (2003) A new approach to spike sorting for multi-neuronal activities recorded with a tetrode—how ICA can be practical. *Neurosci Res* 46:265–272.
- Takahashi S, Sakurai Y. (2009) Sub-millisecond firing synchrony of closely neighboring pyramidal neurons in hippocampal CA1 of rats during delayed non-matching to sample task. *Front Neural Circuits* 3:9.
- Terada S, Sakurai Y, Nakahara H, Fujisawa S. (2017) Temporal and rate coding for discrete event sequences in the hippocampus. *Neuron* 94:1248–1262.
- Tort ABL, Komorowski R, Eichenbaum H, Kopell N. (2010) Measuring phase-amplitude coupling between neuronal oscillations of different frequencies. *J Neurophysiol* 104:1195–1210.
- Tort ABL, Komorowski RW, Manns JR, Kopell NJ, Eichenbaum H. (2009) Theta–gamma coupling increases during the learning of item-context associations. *Proc Natl Acad Sci* 106:20942–20947.
- Tort ABL, Kramer MA, Thorn C, Gibson DJ, Kubota Y, Graybiel AM, Kopell NJ. (2008) Dynamic cross-frequency couplings of local field potential oscillations in rat striatum and hippocampus during performance of a T-maze task. *Proc Natl Acad Sci* 105:20517–20522.
- van Wingerden M, van der Meij R, Kalenscher T, Maris E, Pennartz CMA. (2014) Phase-amplitude coupling in rat orbitofrontal cortex discriminates between correct and incorrect decisions during associative learning. *J Neurosci* 34:493–505.
- Wood ER, Dudchenko PA, Robitsek RJJ, Eichenbaum H. (2000) Hippocampal neurons encode information about different types of memory episodes occurring in the same location. *Neuron* 27:623–633.
- Yamamoto J, Suh J, Takeuchi D, Tonegawa S. (2014) Successful execution of working memory linked to synchronized high-frequency gamma oscillations. *Cell* 157:845–857.
- Zheng C, Bieri KW, Hsiao YT, Colgin LL. (2015) Spatial sequence coding differs during slow and fast gamma rhythms in the hippocampus. *Neuron* 89:398–408.
- Zheng C, Bieri KW, Trettel SG, Colgin LL. (2015) The relationship between gamma frequency and running speed differs for slow and fast gamma rhythms in freely behaving rats. *Hippocampus* 25:924–938.
- Zheng J, Anderson KL, Leal SL, Shestyuk A, Gulsen G, Mnatsakanyan L, Vadera S, Hsu FPK, Yassa MA, Knight RT, Lin JJ. (2017) Amygdala–hippocampal dynamics during salient information processing. *Nat Commun* 8:14413.

(Received 28 January 2019, Accepted 25 May 2019)  
(Available online xxxx)